

Surface integrity generated with peripheral milling and the effect on low-cycle fatigue performance of aeronautic titanium alloy Ti-6Al-4V

D. Yang

School of Mechanical Engineering
Shandong University
Jinan, China
Department of Mechanical Engineering
Anhui University
Hefei
China

Z. Liu

melius@sdu.edu.cn

School of Mechanical Engineering
Shandong University
Jinan
China

ABSTRACT

Machining-induced surface integrity has an important effect on reliability and service life of the components used in the aerospace industry where titanium alloy Ti-6Al-4V is widely applied. Characterisation of machining-induced surface integrity and revealing its effect on fatigue life are conducive to structural fatigue life optimisation design. In the present study, surface topography, residual stress, microstructure and micro-hardness were first characterised in peripheral milling of titanium alloy Ti-6Al-4V. Then, low-cycle fatigue performances of machined specimens were investigated on the basis of the tension-tension tests. Finally, the effects of surface integrity factors (stress concentration factor, residual stress and micro-hardness) on fatigue performances were discussed. Results show that stress concentration can reduce the fatigue life while increasing the residual compressive stress, and micro-hardness is beneficial to prolonging the fatigue life, but when the surface material of the specimen is subjected to plastic deformation due to yield, the residual stress on the surface is relaxed, and the effect on the fatigue performance is disappeared. Under the condition of residual stress relaxation, the stress concentration factor is the main factor to determine the low-cycle fatigue life of titanium alloy Ti-6Al-4V. While for the specimens with no residual stress relaxation,

micro-hardness was the key factor to affect the fatigue life, followed by residual stress and stress concentration factor, respectively.

Keywords: surface integrity; peripheral milling; low-cycle fatigue; Ti-6Al-4V

NOMENCLATURE

R_a	profile average height (μm)
R_y	maximum peak-to-valley profile height (μm)
R_z	average maximum height of the profile (μm)
S_a	residual surface average height (μm)
S_y	maximum peak-to-valley surface height (μm)
S_z	average maximum height of the residual surface (μm)
K_t	stress concentration factor
ρ	notch root radius (μm)
v_c	Cutting speed (m/min)
f_z	feed rate (mm/z)
a_e	radial depth of cut (mm)
σ_{11}	residual stress in cutting direction (Mpa)
σ_{22}	residual stress in the direction that perpendicular to the cutting direction (Mpa)
$ \sigma_{rs} $	mean value of residual stress (Mpa)
N_f	low-cycle fatigue life
$HV_{0.05}$	micro-hardness (Mpa)

1.0 INTRODUCTION

Low weight, high specific strength and other excellent properties make titanium alloy Ti-6Al-4V have wide applications in manufacturing advanced engineering components, such as aero engine casing and impeller blade. Reliability and service life are particularly important for these components. As a consequence, the requirement of machining-induced surface integrity is upgraded. Furthermore, the relationship between machining-induced surface integrity and fatigue performance should be characterise for structural fatigue life optimisation design.

Surface topography introduces stress concentration on the free surface that accelerates crack initiation and propagation compared to a relatively smooth surface⁽¹⁾. Two-dimensional roughness parameters, R_a (arithmetic average roughness), R_y (peak-to-valley height roughness) and R_z (average peak-to-valley height), are always associated with fatigue performance⁽²⁾. All three parameters provide a simple and useful means of quantifying profile height distributions, but they should not be used on an individual basis for estimating fatigue performance. Therefore, it makes sense for the relationship between surface topography and fatigue performance of metals to be expressed in terms of stress concentration factor, K_t ⁽³⁾. Arola and Ramulu suggested a stress concentration factor, $K_t = 1 + 2R_aR_y(\rho R_z)^{-1}$, where ρ is notch root radius⁽⁴⁾. Fatigue life model based on K_t is more accurate than that based on a single roughness parameter⁽⁵⁾.

Having compressive residual stress is shown to have a positive effect on prolonging service life of the component, while tensile residual stress plays an opposite role⁽⁶⁾. Hence, it is

important to obtain the compressive residual stress, and to explore the response relationship between residual stress and fatigue performance under different machining conditions. Zlatin and Field showed that the compressive residual stress is generated in gentle milling, while the tensile residual stress is always in abusive milling⁽⁷⁾. Sridhar et al. found that by increasing the cutting speed, more compressive residual stress was generated in milling IMI-834⁽⁸⁾. Yet Guerville et al. drew quite the opposite conclusion that more tensile residual stress was found with increasing the cutting speed⁽⁹⁾. It is difficult to obtain consensual conclusions due to the high uncertainty of the experimental process and the different properties of workpiece materials. Few researches in the current literature relate residual stress induced by peripheral milling of titanium alloy Ti-6Al-4V and its effect on fatigue performance.

Apparently relationships between microstructural features and fatigue performances of titanium alloys are hard to characterisedue to the fact that these alloys have an extremely complicated microstructure⁽¹⁰⁾. The microstructure of Ti-6Al-4V encompasses a large scale of grain size that can vary significantly under different cutting conditions. As a comprehensive characterisation of the microstructure of the surface material, micro-hardness can be used to characterise the effect of microstructural features on fatigue performance. Relevant researches showed that a certain increase in the hardness over a certain range helps to prolong the fatigue life of components on high cycle fatigue⁽¹¹⁻¹⁴⁾. Nevertheless, machining-induced surface integrity is crucial to fatigue cumulative damage in low-cycle fatigue. The role that variations in the Ti-6Al-4V micro-hardness have on variation in the low-cycle fatigue performance is not very well understood.

The goal of this work is to identify a relationship between surface integrity, milling process parameters and fatigue behaviour of Ti-6Al-4V. Three aspects are contained in the present study as follows: First, surface integrity including surface topography, residual stress, microstructure and micro-hardness was characterised in peripheral milling of titanium alloy Ti-6Al-4V; second, low-cycle fatigue performance of machined specimens was studied on the basis of the tension-tension tests; third, the effects of surface integrity factors (stress concentration factor, residual stress and micro-hardness) on fatigue performances were discussed.

2.0 EXPERIMENTAL WORK

2.1 Workpiece material

The material studied was $\alpha + \beta$ two phase titanium alloy Ti-6Al-4V, which was formed by the free forging and re-crystallisation annealing process. Microstructural features photographed by the Scanning Electron Microscope (SEM) is shown in Fig. 1, the original microstructure of the material, primary α grains as those that are lower in grayscale intensity and the lamellar $\alpha + \beta$ colonies as those areas higher in grayscale intensity. β phase was a boundary phase which was attached to the α matrix with a small amount. The volume fraction of β phase of as-received material is 13.5%, and the chemical compositions of both phases are listed in Table 1.

2.2 Specimen preparation

Figure 2 shows the sketch of the fatigue specimen. Surface A, the investigated surface, is machined using peripheral milling. The machining experiments were carried out on a vertical-type machining centre (DAEWOOACE-V500). Milling tools materials were cemented carbides with 4-flute tool with variable helix angles (38° and 41°). The diameter of the cutter

Table 1
Chemical compositions of α and β phases of Ti-6Al-4V alloy studied

Element		Ti	Al	V	O	C	N
%Weight	α phase	89.29	6.36	3.93	0.16	0.011	0.0011
	β phase	89.16	5.83	4.91	0.08	0.016	0.003

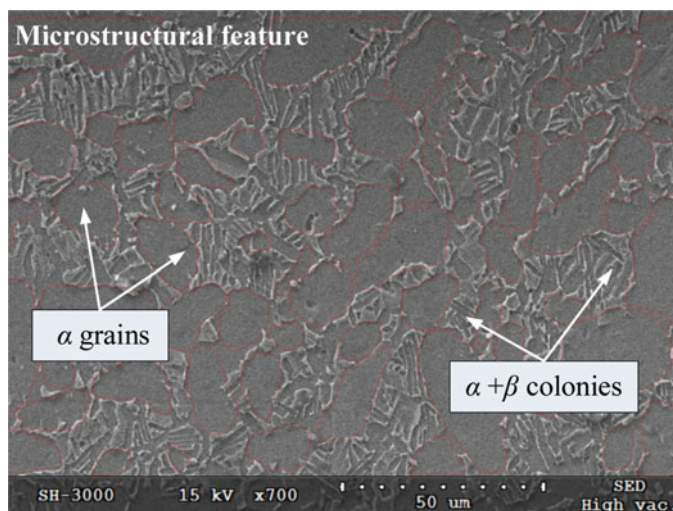


Figure 1. (Colour online) Microstructural feature of Ti-6Al-4V alloy studied.

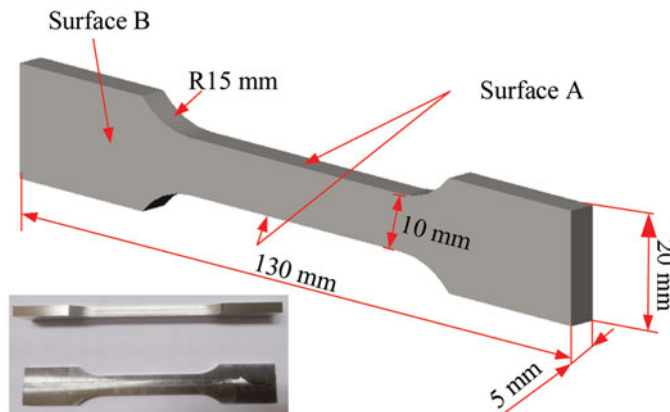


Figure 2. (Colour online) Sketch of the fatigue specimen.

was 6 mm. The milling mode was down milling. Each test specimen was machined with a new tool to exclude the impact of tool wear. The tests were performed with dry machining due to concern regarding the safety of the environment. Surface B is processed by end milling, grinding and polishing.

Table 2
Orthogonal experiment table

Levels/ Factors	Cutting speed v_c (m/min)	Feed rate f_z (mm/z)	Radial depth of cut a_e (mm)
Level 1	20	0.02	0.5
Level 2	50	0.03	1.0
Level 3	80	0.04	1.5
Level 4	110	0.05	2.0

In order to obtain different surface integrity of surface A, orthogonal experimental design method was applied, and 16 groups of experiments were carried out. Cutting speed v_c , feed rate f_z and radial depth of cut a_e are given in Table 2.

2.3 Measurement of surface integrity

2.3.1 Surface topography

Surface topography of surface A was measured using an optical microscope KEYENCE VR-3000. The valuation area was set at 2.6 mm × 1.0 mm. 2D parameters of R_a (profile average height), R_y (maximum peak-to-valley profile height), R_z (average maximum height of the profile) and 3D parameters of S_a (residual surface average height), S_y (maximum peak-to-valley surface height), S_z (average maximum height of the residual surface) were studied. These parameters were taken at three locations and repeated twice at each location on the face of the machined surface, and then the average values were obtained.

2.3.2 Residual stress

For polycrystalline materials, corresponding macro strain of residual stress was considered to be the sum of lattice strain. As a consequence, residual stress can be calculated by measuring lattice strain on the basis of the Hooke's law and the theory of elastic mechanics. The X-ray diffraction method, which is based on the Bragg's law, expressed as Equation (1), is able to fulfill the task

$$n\lambda = 2d \sin \theta, \quad \dots (1)$$

where n is an integer representing the order of diffraction, λ is the wavelength of x-ray, d is the interplanar spacing of crystal planes, and θ is the diffraction angle.

A Proto-LXRD diffractometer with Cu $K\alpha$ radiation tube was used to measure the machining-induced residual stresses. Residual stresses of surface A were measured in two directions: parallel (σ_{11}) and perpendicular (σ_{22}) to the cutting direction in the machined surface. The testing standard is ASTM E915-2010⁽¹⁵⁾, using the $\sin^2\psi$ method, where ψ is the tilt angle of stress coordinates for normal direction of the diffraction plane. The basic testing parameters of the residual stress are listed in Table 3.

2.3.3 Micro-hardness

Micro-hardness on and below the machined surface (Surface B) were measured using micro-hardness tester HVS-1000, and the test load was 0.05kg. Below the machined surface,

Table 3
Basic testing parameters of residual stress

Parameters	Set values
Collimator diameter	1mm
Target	Cu K α
Peak position 2θ	139.47°
Crystallographic planes	213
ψ angles range	$\pm 45^\circ$
Rotation angle	0,90°
Tube voltage	30kV
Tube current	25mA
X-ray elastic constants S_1	$-2.83 \times 10^{-6} \text{ MPa}^{-1}$
X-ray elastic constants $S_2/2$	$11.89 \times 10^{-6} \text{ MPa}^{-1}$

measurements were taken at 20- μm intervals with a depth of 200 μm . Five locations at each specimen were measured, and the average values were employed.

2.3.4 Microstructure

Mosaic block was made to identify the microstructural features on the machined surface (Surface A). Specimens were ground, polished, and then etched in 5 ml HNO₃ (65% conc.) + 3 ml HF (40% conc.) + 100 ml H₂O at room temperature for 10 seconds⁽¹¹⁾. A SAE-3000M SEM was utilised to picture microstructures.

2.4 Fatigue test set-up

Stress-controlled low-cycle fatigue tests were performed on an Instron 8801 electro-hydraulic fatigue testing machine. Servo-hydraulic and servo electric machines were employed for the tests to generate a sinusoid waveform with a frequency of 20Hz. All tests were performed under constant amplitude force control at room temperature utilising a stress ratio of $R = 0.1$. The maximum stress was set to 1,000 MPa, which is slightly above the yield strength of as-received material Ti-6Al-4V at room temperature (894-903 MPa), and all fatigue tests were compliant with BS 3518-1:1993 (Method of fatigue testing). Tests were stopped when the specimen broke, and the tensile-tensile fatigue testing set-up and conditions are listed in Fig. 3.

3.0 RESULTS AND DISCUSSION

3.1 Surface integrity and fatigue performance

3.1.1 Surface topography

In Fig. 4, the surface topology induced by the peripheral milling can be observed. Uniform space ridges along the feed direction can be found. These ridges are caused by the relative movements of the cutter and specimen resulted in the final surface topography, which explicitly reflects the movement track of cutting edge.

For the fact that the calculation process of 3D surface topography parameters considered more features of the machined surface, including surface defects as adhered material particles,

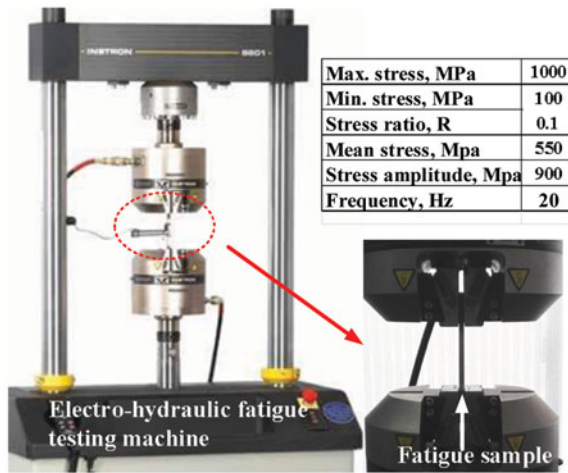


Figure 3. (Colour online) Tensile-tensile fatigue testing set-up and conditions.

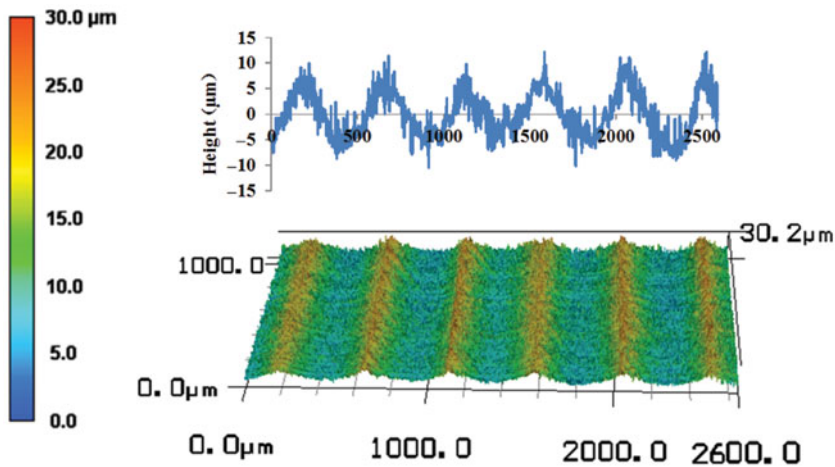


Figure 4. (Colour online) Features of surface topography induced by peripheral milling ($v_c = 50$ m/min, $f_z = 0.05$ mm/z, $a_e = 2.0$ mm).

tearing surface, and debris of microchips, etc. The magnitude of the 3D surface topography parameters is greater than the magnitudes of the corresponding 2D parameters. It was validated by Fig. 5, the effect of cutting conditions on machined surface roughness. In Fig. 5, it can also be found that 3D parameters showed almost the same trend as 2D parameters under different cutting conditions. Seen from Figs 5(a)–5(c), an increase of cutting speed caused a decrease of R_a , R_y , R_z (S_a , S_y , S_z). This is probably due to the fact that more cutting heat was taken away by chips and the built-up edge was reduced. The feed rate effect on the surface roughness value in Figs 5(b)–5(e) showed that it almost linearly increased with the increased feed rate. As for the effect of radial depth of cut in Figs 5(g)–5(i), surface roughness trends showed concave features, while convex for S_z .

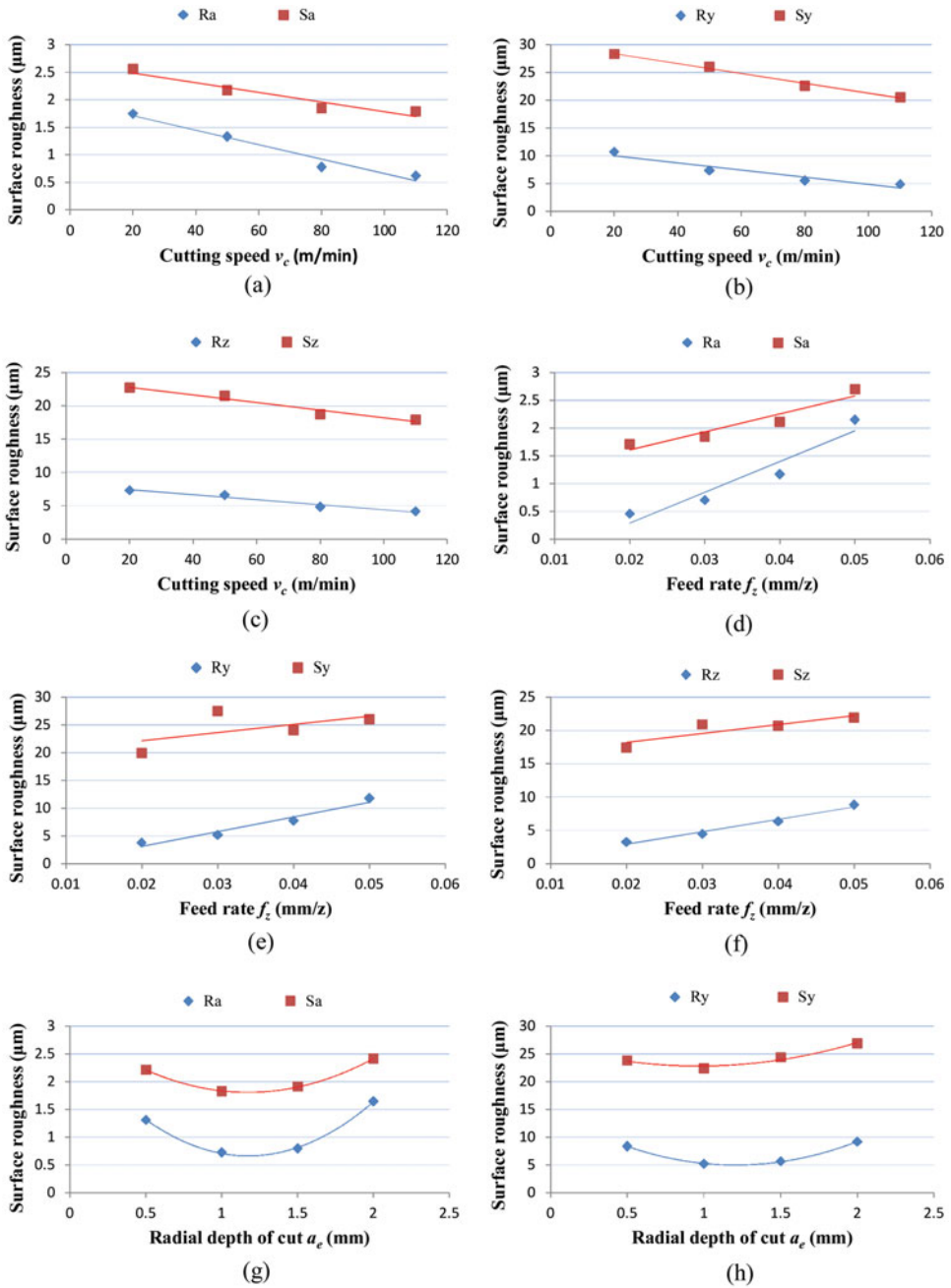


Figure 5. (Colour online) Effect of cutting conditions on machined surface roughness.

3.1.2 Residual stress

The degree of thermal and mechanical work associated with cutting is decisive of the residual stress form at the machined surface⁽¹⁶⁾. In the present study, residual stresses are compressive stresses at the machined surface. That is mainly because more mechanical work was generated

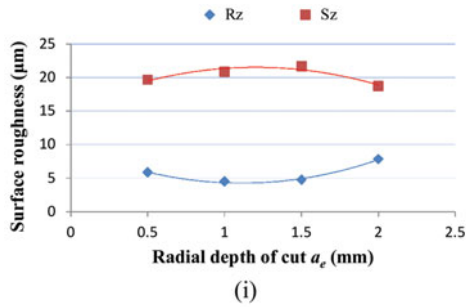


Figure 5. (Colour online) Continued

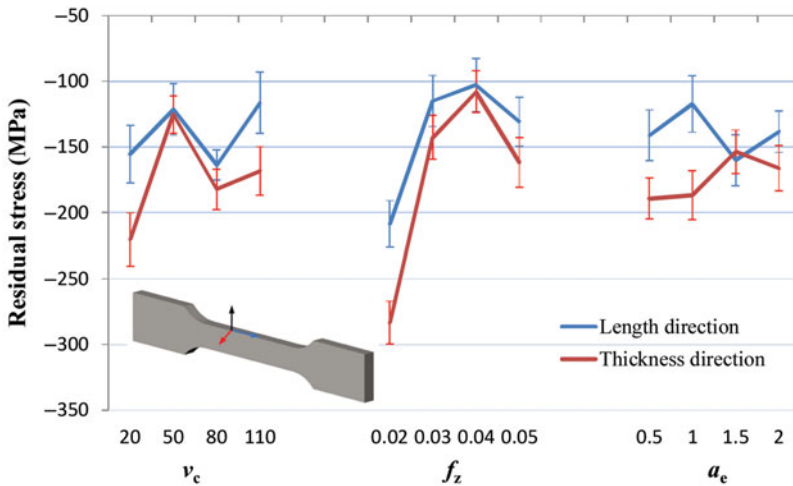


Figure 6. (Colour online) Response relationships between surface residual stress and cutting conditions.

during the machining process. In the case of the higher cutting speed and feed rate, more heat is generated. As a consequence, the mathematical value of compressive stress will decrease. As shown in Fig. 6, the response relationships between surface residual stress and cutting conditions, residual stresses in length and thickness directions present almost the same trend with the variation of cutting conditions. Increasing the cutting speed and feed rate decreases the magnitude of the values of the compressive stress, while the radial depth of cut had no obvious effect on the magnitude of compressive stress. It can also be seen in Fig. 6 that there are large standard deviations in residual stress measurements and four main kinds of errors such as calculation error, sample acceptance error, instrument measurement error, and operation error are responsible for this phenomenon. In order to reduce the influence of test errors on the reliability of fatigue analysis results, the average value of the measured residual stresses was applied in the study.

3.1.3 Micro-hardness

Due to the mechanical effect and the heat generation at the shear zone, work-hardening combining with surface-softening occurred on the machined surface at the same time.

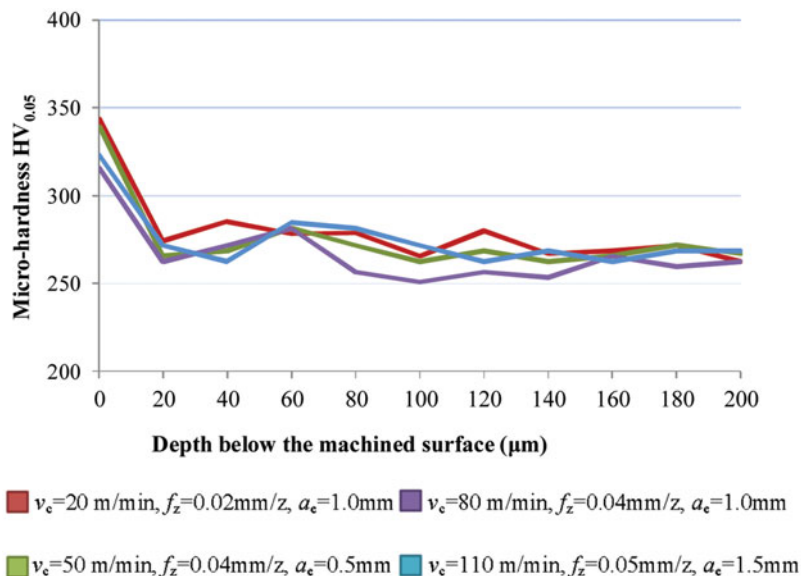


Figure 7. (Colour online) Micro-hardness profiles below the machined surface.

However, it is unable to define the extent of the hardening and softening effect according to the existing literature. Under the conditions of the present study, obvious work-hardening was observed on the machined surface. Hardening rates were in the range of 13.6% to 43.4%. Figure 7 shows micro-hardness profiles below the machined surface of partial specimens.

3.1.4 Microstructure

In the aspect of microstructural features of machined Ti-6Al-4V, lamellar $\alpha + \beta$ colonies were regarded as a unit. And then profiles of α phase were picked up using Image-Pro-Plus software. Size distribution and average diameter of α grains were evaluated.

Figure 8 shows the microstructures and α grain size distributions of the original material and the machined surface under different cutting conditions. α grain diameters of the original material ranged from $6 \mu\text{m}$ to $24 \mu\text{m}$, and the average value is $11.7 \mu\text{m}$. Grain refinement of α grain was noticed at the machined surface under different cutting conditions. The grain refinement rate, which is defined as the ratio of grain size changes to the initial grain size, under the cutting condition of (b), (c) and (d) in Fig. 8 were 30.34%, 29.1% and 27.35%, respectively. Meanwhile, with the decrease in the size of α grain diameter and the increase in the number of α grain, the volume fraction of the boundary phase (β phase) was found increased through visual observation.

Based on the orthogonal experimental analysis method, the response relationships between the grain refinement rate and the cutting conditions were obtained in Fig. 9. In the range of experimental parameters, the α grain refinement rate decreased distinctly with the increase of cutting speed but slightly increased with the increase of the feed rate. The parameter of the depth of cut played an opposite role in increasing the grain refinement rate.

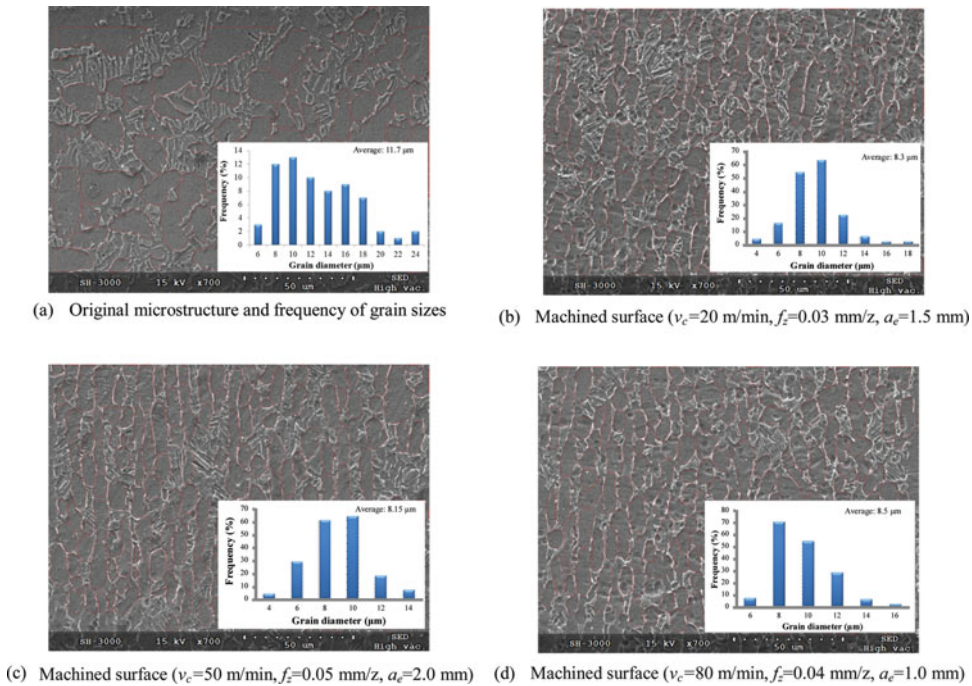


Figure 8. (Colour online) Microstructure and α grain size distribution of the original material and the machined surface.

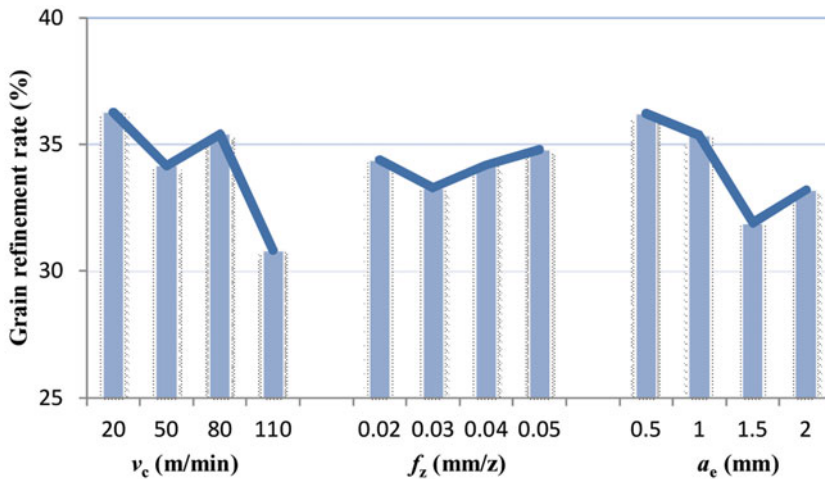


Figure 9. (Colour online) Response relationships between α grain refinement rate and cutting conditions.

3.1.5 Low-cycle fatigue performances

For all the specimens studied, the numbers of cycles to failure were in the range of 2,510 to 8,141. Forty-five-degree shear fracture surfaces were formed on the fractured specimens. That is because the slip systems are in the best orientation on these surfaces. The main deformation

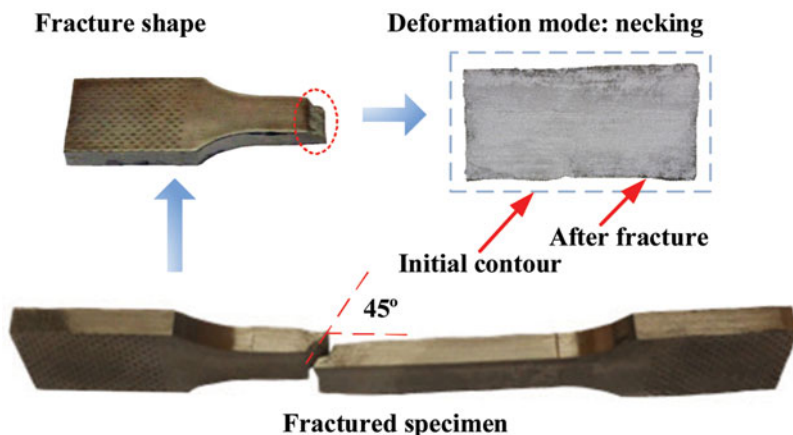


Figure 10. (Colour online) Features of the fractured specimen.

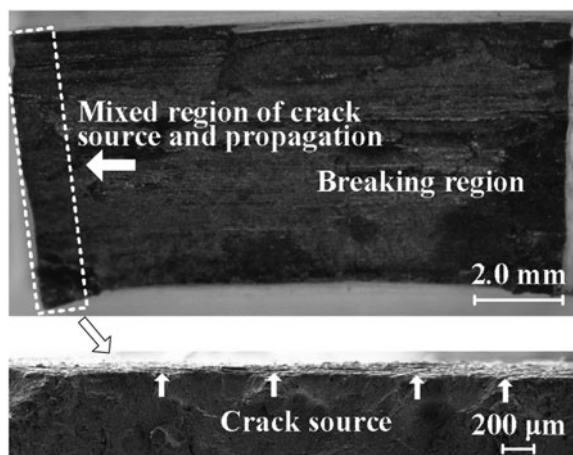


Figure 11. Macroscopic fracture morphology of Ti-6Al-4V.

mode of the test specimens is necking, and the reduction ratio of areas was up to 30.2%. All these phenomena were shown in Fig. 10.

Figure 11 shows the typical macroscopic fracture morphology of Ti-6Al-4V under tensile-tensile fatigue tests. High alternate stress in the low-cycle fatigue tests caused the fatigue crack size to quickly reach the critical value and produced an instantaneous fracture. As a consequence, the crack propagation region was not large, and there was not a sharp division between the fatigue crack source region and the crack propagation region. In the mixed region of crack source and propagation, multi-sources were observed, and multiple stress concentration is the main reason for this phenomenon.

Figure 12 shows the typical microscopic fracture morphology of Ti-6Al-4V under tensile-tensile fatigue tests. The fatigue-crack source region is the earliest fracture, where crack propagation rate is slow. Repeated friction occurred during the crack opening and closing with loading cycles in this region. As a consequence, the fatigue-crack source region looks neat and smooth. Moreover, slip lines and elongated dimples were observed in the mixed

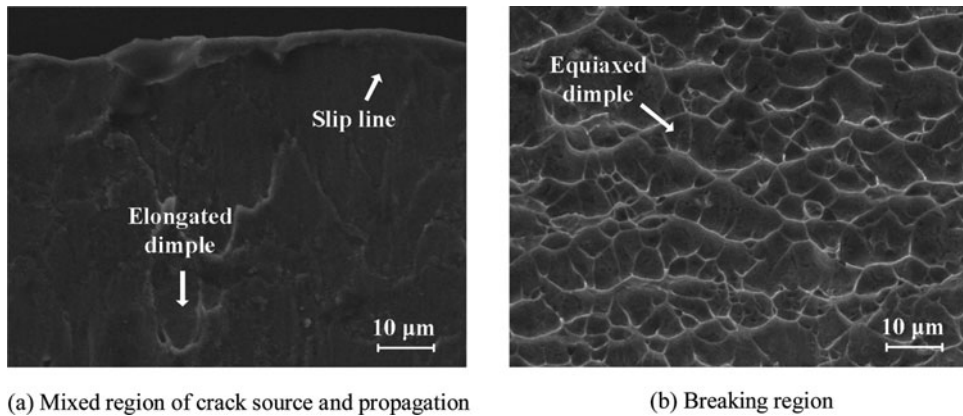


Figure 12. Microscopic fracture morphology of Ti-6Al-4V.

region of crack source and propagation. Breaking region showed the transient characteristic of the static load. Equal-axis dimples were finally generated on the fracture surface.

3.2 Influence of surface integrity on fatigue performance

Stress concentration factor K_t , mean value of residual stress $|\sigma_{rs}|$ and micro-hardness $HV_{0.05}$ were selected as the three main factors to evaluate the influence of surface integrity on low-cycle fatigue life, N_f . Details of these factors are listed in Table 4.

Based on the surface integrity factors and fatigue life data, the response curves between K_t , $|\sigma_{rs}|$, $HV_{0.05}$ and N_f are shown in Fig. 13.

Under high alternate stress of the low-cycle fatigue tests, plastic deformation occurred and strain superimposed gradually (Ratchet effect) on the material surface. As a consequence, the influence of surface topography on the fatigue performance is changed from stress concentration to strain concentration, and the influence of the stress concentration factor on the low-cycle fatigue life is weakened. However, strain concentration on the surface of the specimen is the same as that in the stress concentration area, the stress concentration factor, which takes into account the characteristics of the surface topography, can also be used to reflect the state of strain concentration. Even if the degree of stress concentration is reduced, it still has an effect on low-cycle fatigue performance. Figure 13(a) shows that fatigue life decreased slightly with the increase of the stress concentration factor K_t .

The residual stress state induced by machining plays a dominant role in extending or shorting the fatigue performance of metallic materials, while residual stress relaxes significantly or even completely under high-loading conditions and the effect on the fatigue performance is weakened or disappeared. According to the relaxation criterion, the residual stress will be relaxed only when the total load, which is the superposition of the maximum value of the alternating load and the residual stress value, is greater than the yield limit of the material. As seen from Table 2, part of the specimen is under the alternating loads to meet the stress state of the residual stress relaxation conditions and there is also a part of the specimen without relaxation due to the large residual stress, such as specimen A01, A02, A03, A05, A09, A10, A12, A13 and A16. As shown in Fig. 13(b), the fatigue performance of the fatigue specimens with the occurrence of residual stress relaxation and no relaxation was different. For the specimens with residual stress relaxation, the residual stress has no significant effect on the low-cycle fatigue performance (Trend line 1), while for the specimens

Table 4
Surface integrity factors and fatigue life data

NO.	Cutting parameters			Key factors of surface integrity							Fatigue life
	v_c m/min	f_z mm/z	a_e mm	R_a μm	R_y μm	R_z μm	ρ μm	K_t	σ_{rs} Mpa	HV _{0.05} Mpa	N_f
A01	20	0.02	1.0	0.50	4.03	3.07	1.50	1.547	-170.3	344	7502
A02	20	0.03	1.5	1.01	6.85	5.67	2.50	1.371	-129.8	337	4441
A03	20	0.04	2.0	2.20	12.88	9.90	3.73	1.807	-109.1	344	5787
A04	20	0.05	0.5	3.27	18.89	10.61	7.08	1.786	-91.8	348	4118
A05	50	0.02	1.5	0.37	3.08	2.81	0.99	1.810	-129.5	319	7479
A06	50	0.03	1.0	0.68	4.75	4.36	2.05	1.215	-61.7	339	7169
A07	50	0.04	0.5	1.10	6.99	6.18	1.84	2.117	-53.2	312	5046
A08	50	0.05	2.0	3.18	14.49	13.06	4.76	1.696	-84.5	313	5141
A09	80	0.02	2.0	0.56	4.64	4.17	1.62	1.380	-179.4	330	4940
A10	80	0.03	0.5	0.48	4.20	3.68	1.69	1.246	-118.9	340	5735
A11	80	0.04	1.0	0.82	5.77	5.12	1.92	1.482	-61.3	316	4651
A12	80	0.05	1.5	1.26	7.38	6.30	2.37	1.662	-101.8	312	2922
A13	110	0.02	0.5	0.39	3.28	2.87	1.37	1.383	-176.7	344	8141
A14	110	0.03	2.0	0.64	4.71	4.12	1.47	1.671	-33.2	329	7695
A15	110	0.04	1.5	0.55	5.14	4.16	1.50	1.570	-57.4	341	5167
A16	110	0.05	1.0	0.89	6.25	5.45	1.77	1.719	-112.0	333	2510

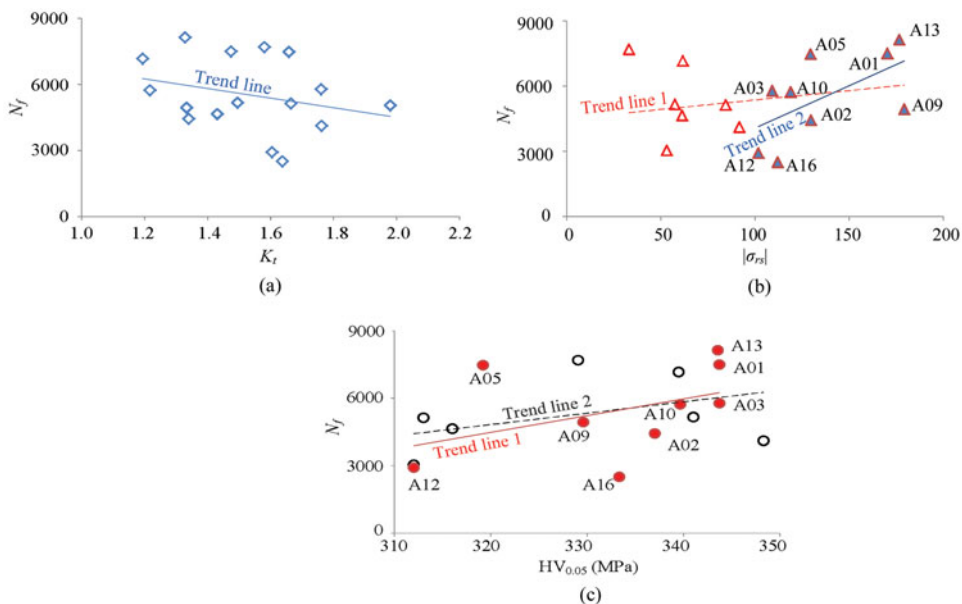


Figure 13. (Colour online) Response curves between K_t , $|\sigma_{rs}|$, $HV_{0.05}$ and N_f .

with no stress relaxation, the low-cycle fatigue life increases obviously with the increase of residual compressive stress (Trend line 2).

Micro-hardness is the result of the combination of strain hardening and thermal softening. It is also a comprehensive characterisation of the microstructure of the surface material. With the increase of the micro-hardness of the machined surface, the plasticity and toughness of the surface layer decrease, and the surface crack is suppressed. Even in the presence of micro-cracks on the machined surface, the increase of yield limit of the surface material makes the expansion of micro-cracks need more stress values and more cycles. Therefore, the increase of micro-hardness will lead to the improvement of the fatigue life. Under the high alternate stress of low-cycle fatigue tests, for the plastic flow of the surface material, the effect of micro-hardness on the low-cycle fatigue life is not significant, as described by trend line 2 in Fig. 13(c), and the improvement of micro-hardness can be improved for the specimen without residual stress relaxation, as described by trend line 1.

On the basis of the above analysis, the influence of the key factors of surface integrity on the low-cycle fatigue performance of the specimens can be divided into two cases: residual stress relaxation and no relaxation. According to the data of surface integrity and low-cycle fatigue life, the linear regression analysis method is used to establish the empirical model of low-cycle fatigue life in two cases:

Residual stress relaxation,

$$N_f = 10^{2.2503} K_t^{-1.3779} HV_{0.05}^{0.6851} \quad \dots (2)$$

Without residual stress relaxation,

$$N_f = 10^{-6.7537} K_t^{-0.4113} |\sigma_{rs}|^{1.0839} HV_{0.05}^{3.2069} \quad \dots (3)$$

Under the condition of residual stress relaxation, the influence of the stress concentration factor on the low-cycle fatigue life of the machined surface is higher than that of the micro-hardness, which is the main factor to determine the low-cycle fatigue life of titanium alloy Ti-6Al-4V. For the specimens with no residual stress relaxation, the higher the residual compressive stress, the higher the fatigue life, and the influence of residual stress on fatigue life is only lower than that of micro-hardness, which is higher than that of stress concentration factor.

4.0 CONCLUSION

For the purpose of improving the reliability and prolonging the service life of Ti-6Al-4V components, machining-induced surface integrity and its effect on fatigue life are investigated. Indicators such as stress concentration factor that calculated by surface roughness parameters, residual stress, microstructure and micro-hardness are included. Conclusions can be summarised as follows:

The values of 3D surface topography parameters are larger than those of 2D ones, while both kinds of parameter values showed almost the same change trend with different cutting conditions. The values of surface roughness are proportional to cutting speed, and inversely proportional to feed rate. The radial depth of cut has no significant effect on surface roughness. Residual stresses are compressive stresses at the machined surface in the present study. Increasing the cutting speed and feed rate decreased the mathematical values of compressive stress. Radial depth of cut had no obvious effect on the magnitude of compressive stress.

Work-hardening was observed on the machined surface and the hardening rates were in the range of 13.6% to 300 43.4%. The α grain refinement rate decreased distinctly with the increase of cutting speed but slightly increased with the increase of feed rate. Radial depth of cut played an opposite role in increasing the grain refinement rate.

The results of tensile-tensile fatigue tests show that the numbers of cycles to failure were in the range of 2510 to 8141. The main deformation mode of the test specimens is necking, and the reduction ratio of areas was up to 30.2%. Widths of crack source and propagation regions are small due to the large stress amplitude. Slip lines and elongated dimples were observed in the mixed region of crack source and propagation. The equal-axis dimple is a typical feature on the fracture surface.

Stress concentration can reduce the fatigue life, while the stress concentration factor cannot express the low-cycle fatigue performance significantly due to the ratchet effect. Increasing the residual compressive stress and micro-hardness is beneficial to prolonging the fatigue life, but when the surface material of the specimen is subjected to plastic deformation due to yield, the residual stress on the surface is relaxed, and the effect on the fatigue performance has disappeared. Under the condition of residual stress relaxation, the stress concentration factor is the main factor to determine the low-cycle fatigue life of titanium alloy Ti-6Al-4V. For the specimens with no residual stress relaxation, the influence of residual stress on fatigue life is only lower than that of micro-hardness, which is higher than that of stress concentration factor.

ACKNOWLEDGEMENTS

This work was supported by the National Natural Science Foundation of China (51425503, 51375272, U1201245), Major Science and Technology Program of High-End CNC Machine Tools and Basic Manufacturing Equipment (2014ZX04012014) and grants from Taishan Scholar Foundation (TS20130922).

REFERENCES

1. CHENG, Z. and LIAO, R. Effect of surface topography on stress concentration factor, *Chinese J Mechanical Engineering*, 2015, **28**, (6), pp 1141-1148.
2. WANG, Y., MELETIS, E. I. and HUANG, H. Quantitative study of surface roughness evolution during low-cycle fatigue of 316L stainless steel using scanning whitelight interferometric (SWLI) Microscopy, *Int J Fatigue*, 2013, **48**, pp 280-288.
3. PETERSON, R. E. *Stress Concentration Factors*, 1974, John Wiley and Sons, New York, New York, US.
4. AROLA, D. and RAMULU, M. An examination of the effects from surface texture on the strength of fiber-reinforced plastics, *J Composite Materials*, 1999, **33**, (2), pp 101-186.
5. YAO, C. F., WU, D. X. and JIN, Q. C. Influence of high-speed milling parameter on 3D surface topography and fatigue behavior of TB6 titanium alloy, *Transactions of Nonferrous Metals Society of China*, 2013, **23**, (3), pp 650-660.
6. YAKOVLEV, M. G. Improving fatigue strength by producing residual stresses on surface of parts of gas-turbine engines using processing treatments, *J Machinery Manufacture and Reliability*, 2014, **43**, (4), pp 283-286.
7. ZLATIN, N. and FIELD, M. Procedures and precautions in machining titanium alloys, *Titanium Science and Technology*, 1973, Springer US, Boston, pp 489-504.
8. SRIDHAR, B. R., DEVANANDA, G. and RAMACHANDRA, K. *et al.* Effect of machining parameters and heat treatment on the residual stress distribution in titanium alloy IMI-834, *J Materials Processing Technology*, 2003, **139**, pp 628-634.

9. GUERVILLE, L., VIGNEAU, J. and DUDZINSKI, D. Influence of machining conditions on residual stresses, *Metal Cutting and High Speed Machining*, 2002, Kluwer Academic Plenum Publishers, Netherlands, pp 201-210.
10. LEYENS, C. and PETERS, M. *Titanium and Titanium Alloys*, Wiley-VCH, Weinheim, 2003.
11. SEALY, M. P., GUO, Y. B. and CASLARU, R. C. *et al.* Fatigue performance of biodegradable magnesium–calcium alloy processed by laser shock peening for orthopedic implants, *Int J Fatigue*, 2016, **82**, pp 428-436.
12. SASAHARA, H. The effect on fatigue life of residual stress and surface hardness resulting from different cutting conditions of 0.45% C steel, *Int J Machine Tools and Manufacture*, 2005, **45**, (2), pp 131-136.
13. WU, G. Q., SHI, C. L. and SHA, W. *et al.* Effect of microstructure on the fatigue properties of Ti–6Al–4V titanium alloys, *Materials & Design*, 2013, **46**, pp 668-674.
14. POLASIK, A. The Role of Microstructure on High Cycle Fatigue Lifetime Variability in Ti-6Al-4V, Diss. The Ohio State University, 2014.
15. ASTM E915-10, *Standard test method for verifying the alignment of x-ray diffraction instrumentation for residual stress measurement*, ASTM, 2010.
16. SUNDER, R. Why and how residual stress affects metal fatigue, *Advanced Materials*, 2016, Springer International Publishing, pp 489-504.